

# Subpulse Drifting, Nulling and Mode changing in PSR J1822–2256

Rahul Basu<sup>1</sup>, Dipanjan Mitra<sup>2,3</sup>

<sup>1</sup> *Inter-University Centre for Astronomy and Astrophysics, Pune, 411007, India; rahulbasu.astro@gmail.com*

<sup>2</sup> *National Centre for Radio Astrophysics, Tata Institute of Fundamental Research, Pune 411007, India*

<sup>3</sup> *Janusz Gil Institute of Astronomy, University of Zielona Góra, ul. Szafrana 2, 65-516 Zielona Góra, Poland*

7 July 2019

## ABSTRACT

We report a detailed observational study of the single pulses from the pulsar J1822–2256. The pulsar shows the presence of subpulse drifting, nulling as well as multiple emission modes. During these observations the pulsar existed primarily in two modes; mode A with prominent drift bands and mode B which was more disorderly without any clear subpulse drifting. A third mode C was also seen for a short duration with a different drifting periodicity compared to mode A. The nulls were present throughout the observations but were more frequent during the disorderly B mode. The nulling also exhibited periodicity with a clear peak in the fluctuation spectra. Before the transition from mode A to nulling the pulsar switched to a third drifting state with periodicity different from both mode A and C. The diversity seen in the single pulse behaviour of the pulsar J1822–2256 provides an unique window into the emission physics.

**Key words:** pulsars: general - pulsars: individual: J1822–2256.

## 1 INTRODUCTION

The single pulse sequences from pulsars, particularly the longer period pulsars, show a number of different phenomena like subpulse drifting, nulling and mode changing which are representative of the physical processes responsible for the radio emission. A general model has emerged which explains the generation of ultra-relativistic plasma in the pulsar magnetosphere leading to coherent radio emission (Sturrock 1971; Ruderman & Sutherland 1975; Mitra 2017). In this picture the plasma is believed to originate in the inner acceleration region (IAR) which is characterised by large electric and non-dipolar magnetic fields. Sparking discharges take place due to pair production from  $\gamma$ -ray photons in the large magnetic fields of the IAR resulting in a non-stationary plasma flow. The multi-component relativistic plasma clouds undergo nonlinear instabilities around heights of five hundred kilometers above the stellar surface to form charge separated solitons. The coherent radio emission arises as curvature radiation from the solitons moving in curved magnetic field lines (Asseo & Melikidze 1998; Melikidze *et al.* 2000; Gil *et al.* 2004; Mitra *et al.* 2009). The only source of periodicity in the single pulse dynamics is due to the  $\gamma \mathbf{f} \times \mathbf{B}$  drift in the IAR which is believed to be responsible for subpulse drifting. The other periodic or quasi-periodic phenomena associated with pulsar emission, like nulling and mode changing, are difficult to explain using the above model. The periodic nulling is associated with empty sight line passes between the rotating subbeam system (Herfindal & Rankin 2007). However, in a recent work Basu *et al.* (2017) found that the empty sight line traverse was not adequate to explain the periodic nulling, particularly

in pulsars with core components. It was reported by Basu *et al.* (2016); Mitra & Rankin (2017) that the periodic amplitude modulation is very different from subpulse drifting. As a result Basu *et al.* (2017) suggested that the standard model of emission is no longer adequate to explain the different phenomena seen in pulsars. An additional triggering mechanism from outside the IAR must periodically affect the plasma flow in the pulsar magnetosphere. In this context the coexistence of multiple drifting and non-drifting modes and nulling in the same pulsar is further indication of an external triggering mechanism. Therefore, characterising these phenomena should serve as important inputs into understanding the origin of the triggering mechanism.

There are only a handful of pulsars where multiple drifting states exist in addition to nulling and mode changing. The most well studied pulsar in this group is PSR B0031–07 where the drifting periodicity changes around the nulls (Huguenin *et al.* 1970; Vivekanand & Joshi 1997; Smits *et al.* 2005; McSweeney *et al.* 2017). Similar coexistence of multiple subpulse drifting modes with nulling is seen in the pulsars B1918+19 (Hankins & Wolszczan 1987; Rankin *et al.* 2013), B1944+17 (Deich *et al.* 1986; Kloumann & Rankin 2010), B2319+60 (Wright & Fowler 1981) and B2303+30 (Redman *et al.* 2005). In some of these pulsars the nulling is also periodic in nature (Basu *et al.* 2017). Additionally, pulsars B1918+19 and B1944+17 have also been reported to have non-drifting modes. In the Meterwavelength Single-pulse Polarimetric Emission Survey (Mitra *et al.* 2016; Basu *et al.* 2016, 2017, MSPES) a possible existence of multiple drifting states in addition to nulling was reported for the pulsar J1822–2256. The sub-

pulse drifting and nulling in this pulsar have also been reported by [Weltevrede et al. \(2006, 2007\)](#); [Serylak et al. \(2009\)](#); [Naidu et al. \(2017\)](#). However, the limited lengths of the observations as well as lower sensitivities of the single pulses in these studies did not facilitate a proper characterisation of the emission properties. In this work we have carried out longer duration and more sensitive observations to study the single pulse dynamics in the pulsar J1822–2256. We have characterised with greater accuracy the subpulse drifting, nulling and the mode changes seen in this pulsar. In addition we have also explored the physical processes in the pulsar magnetosphere that can give rise to these variations in the single pulse properties.

## 2 OBSERVATIONS AND ANALYSIS

We have carried out extensive observations of the pulsar J1822–2256 using the Giant Meterwave Radio Telescope (GMRT) located near Pune, India ([Swarup et al. 1991](#)). The GMRT is an interferometric array consisting of thirty antennas each of forty five meter diameter, with fourteen antennas located within a central square kilometer area and the remaining sixteen antennas spread out along three arms in a Y-shaped array. We have used the Telescope in the phased array mode where the signals from different antennas were co-added. In order to reach sufficient sensitivity for single pulse studies we used approximately twenty antennas, including all the available central square antennas and the two nearest arm antennas. A phase calibrator was recorded at the start of the observation as well as every hour and appropriate “phasing” solutions were estimated to correct for temporal gain variations for each antenna. This resulted in phasing breaks between the recorded single pulse sequence. We observed the pulsar on 5<sup>th</sup> November 2015 for approximately three hours. The pulsar has a period of 1.87 seconds which ensured around 5700 single pulses for these studies.

The observations recorded total intensity signals from the pulsar with the maximum frequency set at 339 MHz and spread over 33 MHz bandwidth. In contrast the MSPES carried out full polarization studies with only 16 MHz bandwidth. The increased bandwidth resulted in higher sensitivity detections of the single pulses. However, the polarization information from the earlier observations was also used to investigate the emission properties. The time resolution of the observations was 491.52 microseconds. The known dispersion measure ( $121.20 \text{ pc cm}^{-3}$ ) was used to correct for the temporal spread across the frequency band. Subsequently, the dispersion corrected signals were averaged across all frequencies to produce a series of total intensity measurements from the pulsar for the entire observing duration. During the phasing breaks suitably weighted noise signals were inserted in between the pulsar signal to preserve continuity for fluctuation spectral studies. Finally, a two dimensional pulse stack with one axis along the pulse longitude, separated into integral bins, and the other along the pulse number, was formed from the time series signals. Different analyses for identifying emission modes, measuring subpulse drifting features and nulling were carried out on the pulse stack.

As mentioned earlier due to the increased bandwidth the single pulses were more prominent and we inspected them visually to identify the different emission modes. The subpulse drifting was characterised using the fluctuation spectral analysis ([Backer 1973](#); [Backer et al. 1975](#)). We used the Longitude Resolved Fluctuation Spectra (LRFS) where Fourier transforms across each longitude was carried out for a certain sequence of single pulses. The subpulse drifting periodicities were seen as frequency peaks in the

fluctuation spectra. In addition to the the average LRFS studies we have also determined shorter duration LRFS corresponding to different emission modes. In the MSPES studies proper nulling analysis could not be carried out due to weaker sensitivities of the single pulses. In this work we have utilized the improved sensitivities to carry out a detailed analysis of the null and burst pulses. The techniques used to characterize the nulling behaviour are detailed in [Basu et al. \(2017\)](#). We established energy histograms for the on-pulse and off-pulse regions of the pulsar profile to identify the nulling fractions. Initially the null and burst pulses were identified using statistical boundaries. Subsequently, we visually inspected every null to eliminate any erroneous identification. The null and burst sequences were characterized by the respective null length and burst length histograms. Finally, a sequence of ‘0’ and ‘1’ was setup identifying the null and burst pulses respectively. An FFT was carried out on this sequence to identify any periodicity associated with nulling.

## 3 THE EMISSION MODES AND SUBPULSE DRIFTING

We have identified three distinct emission modes in the pulsar J1822–2256 based on its single pulse properties as shown in figure 1. The primary distinguishing feature amongst the different modes was the nature of subpulse drifting. In the majority of the single pulse sequence we were able to identify the modes by visual inspection. However, in some instances it proved difficult either due to mixing of the modes or reduction in intensity due to scintillation. The most prevalent emission mode was classified as mode A and showed prominent drift bands from the leading to the trailing edge of the pulse window. The corresponding profile in figure 2 (top panel) shows the trailing part to be brighter than the leading part in this mode. Mode A was present for roughly 45 percent of the time during the observing duration. The average length of the mode was 82 periods with the minimum duration being 28 periods and maximum duration being 288 periods. The pulsar transitioned frequently to the second mode B which was more disorderly and did not show any clear drift bands. The profile in figure 2 (middle panel) resembles a double peaked structure much weaker than mode A. Mode B was somewhat less frequent than mode A and was seen in around 38 percent of the single pulses during these observations. The average modal length was 68 periods, with minimum duration of 18 periods and maximum duration of 319 single pulses. Finally, the least frequent but quite distinct mode C also showed prominent drift bands with drifting periodicity different from mode A (see table 1). In this mode the pulsar was brighter towards the trailing part of the profile window as seen in the profile shape (figure 2, bottom panel). The mode was the least frequent and only seen once for around 200 periods which correspond to 4 percent of the observing duration. In addition to the the three distinct modes of emission the pulsar also showed nulling which was spread out throughout the observations but seen more frequently in the weaker B mode. Another different emission feature arose sometimes within mode A before the transition from the drifting state to nulls. The drifting property changed, as shown in figure 3, with the periodicity of subpulse drifting becoming much shorter. However, this lasted for only a short duration each time and was not identified as a separate mode. There was no clear ordering seen in the mode changing between different states. In some instances the pulsar changed from mode A to transition state and then to nulls followed by mode B. At other occasions the transition to mode B did not happen after the nulls and the pulsar reverted back to mode A.

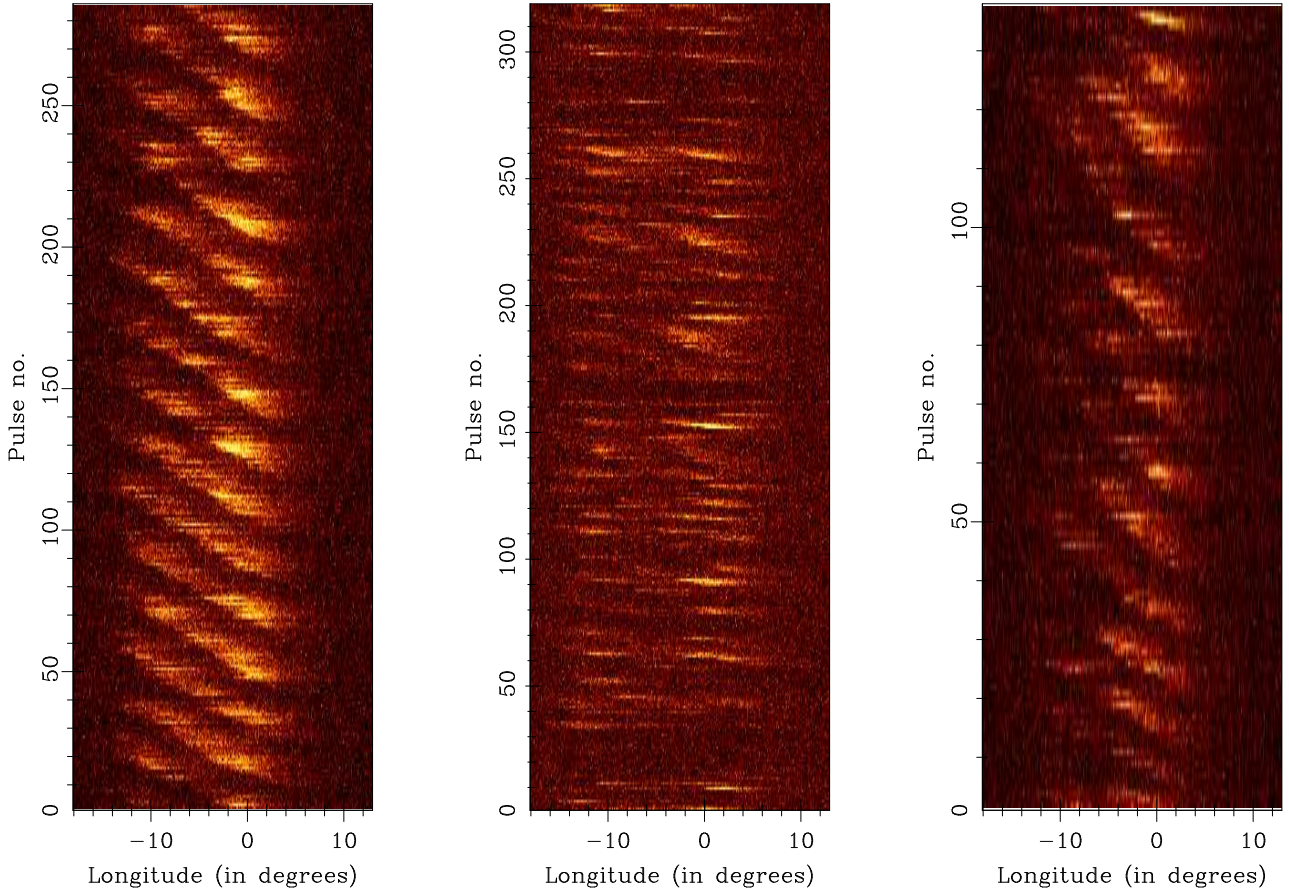


**Figure 1.** The figure shows the three different emission modes seen in the single pulse sequence of PSR J1822–2256. The left panel shows a sequence of mode A between pulse number 2679 and 2963 with regular drift bands. The central panel shows the single pulses from pulse number 3595 to 3912 and corresponds to mode B. This mode does not exhibit any clear subpulse drifting and has more frequent nulls compared to mode A. The right panel shows single pulses between 3018 and 3154 and is identified as mode C. The mode also shows distinct drift bands like mode A but unlike mode A is more prominent towards the trailing edge of the pulse window. The drifting periodicity in mode C is also different from mode A.

**Table 1.** The Subpulse Drifting properties during the different emission modes of PSR J1822–2256.

Mode	$f_p$ (cy/ $P$ )	FWHM (cy/ $P$ )	$S$	$P_3$ ( $P$ )	$P_2$ ( $^\circ$ )
Mean	$0.058 \pm 0.010$	0.023	17.2	$17.1 \pm 2.9$	—
A	$0.051 \pm 0.004$	0.010	61.8	$19.6 \pm 1.6$	$8.3 \pm 0.1$
Trans. (A)	$0.070 \pm 0.009$	0.020	27.4	$14.3 \pm 1.8$	$9.1 \pm 0.1$
C	$0.093 \pm 0.010$	0.023	16.5	$10.7 \pm 1.1$	$7.6 \pm 0.1$

### 3.1 Estimating Drifting properties

We have carried out detailed measurements of the average drifting properties as well as in individual emission modes using the fluctuation spectral analysis. In figure 4 we show the time evolution of the LRFS as detailed in Basu & Mitra (2018). The typical FFT length for each time realisation of the LRFS in these plots was 256 periods. The starting point was shifted by fifty periods and the process was continued till the end of the observing duration.

Each such realisation of the LRFS was averaged across the longitudes and plotted as a function of the starting period. The time averaged LRFS showed the presence of two distinct peaks, one around zero frequency which is associated with nulling, and the second corresponding to the subpulse drifting in the most dominant mode A. It should be noted that during one 256 period cycle, the pulsar is expected to make multiple transitions from mode A, with prominent drifting, to mode B, without any distinct drifting peak. This contributed to the peak amplitude being weaker and the peak more wider than expected from just mode A. The periodicities corresponding to the other drifting states were not seen as separate peaks in the average LRFS due to their low prevalence in the pulse sequence. However, they contributed to the wide structure adjacent to the peak frequency. The variations of the drifting peak across the pulse window are also shown in figure 5. The peak amplitude (top window) showed a double peaked structure with the trailing part twice as high as the leading one. Additionally, the phase variations across the window (middle window) were not linear but were steeper towards the leading part of the profile and became flatter towards the trailing side. The phase variations were large amounting to about  $600^\circ$  across roughly  $20^\circ$  variation in longitude.

In addition we have also isolated single pulse sequences corresponding to the different emission states and determined the fluctuation spectra as shown in figure 6. The figure shows four separate

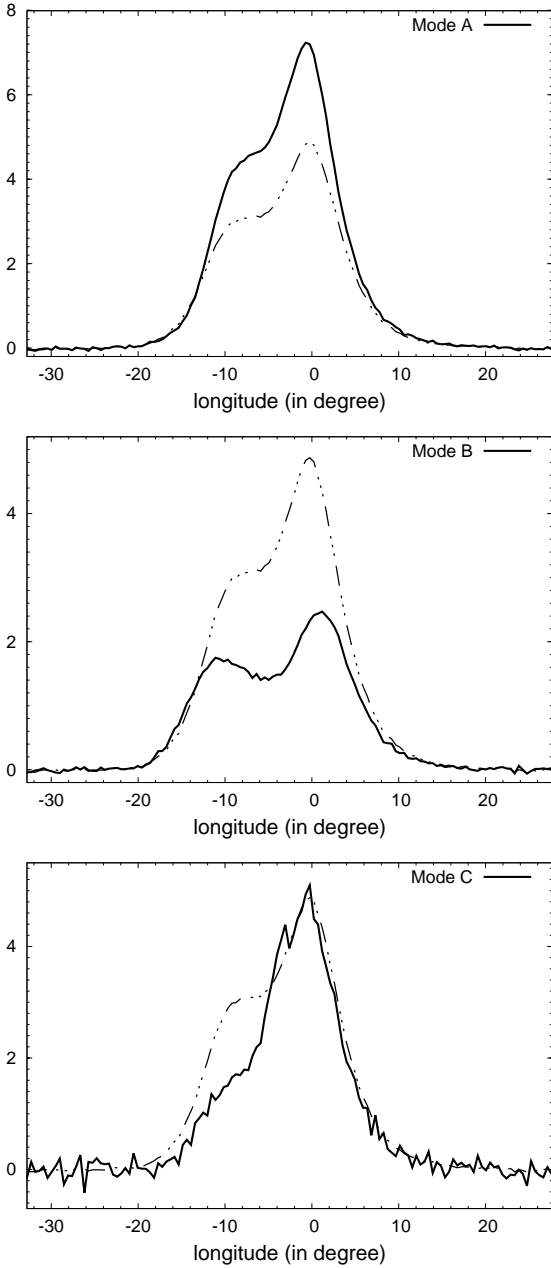


**Figure 2.** The figure shows the variations in the profile shapes in the three distinct emission modes of the pulsar J1822–2256 superposed on the average profile (dot dashed line). The top panel corresponds to mode A with prominent drift bands across the pulse window and is brighter near the trailing side. The middle panel plots the profile of the second mode B which is less bright and do not show any clear drifting pattern. The bottom panel corresponds to mode C which also shows subpulse drifting with different characteristics compared to mode A. The profile indicates that the trailing edge is brighter in this mode.

LRFS, the top left plot corresponding to mode A; the top right plot for a sequence during the transitional drifting state in mode A before the onset of nulling; the bottom left plot shows the LRFS in mode B; and finally the bottom right plot corresponds to the pulse sequence in mode C. We have measured the drifting features in the three sequences where a clear frequency peak could be identified as reported in Table 1. The periodicity in Mode A was  $19.6 \pm 1.6$

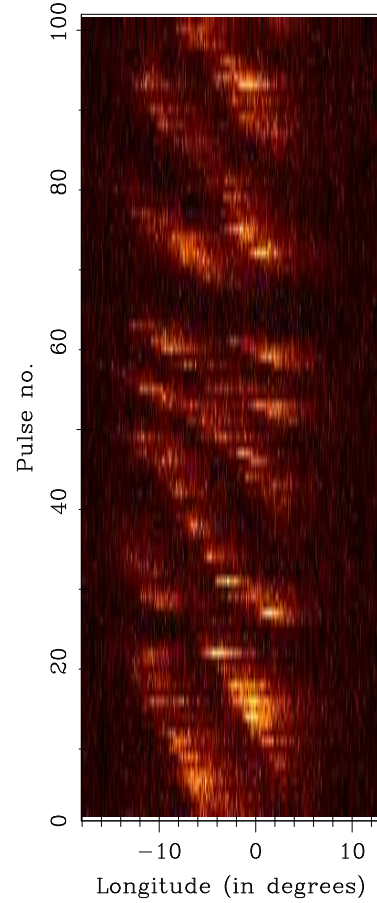


**Figure 3.** The figure shows the distinct behaviour seen sometimes in mode A before the transition to the null state. The drifting nature changes before the onset of the nulls with the periodicity of subpulse drifting becoming much faster. The pulsar recovers to the original drifting state just after nulling.

$P$  which changed to  $14.3 \pm 1.8 P$  before the onset of nulls. Mode C showed a different periodicity of  $10.7 \pm 1.1$ . We do not see any clear harmonical relation between the different periodicities in this pulsar. The LRFS also showed the drifting to be present across the entire pulse profile in mode A but only near the trailing part of the profile in mode C. The strength of the drifting peak was estimated using  $S = V_p/\text{FWHM}$ , where  $V_p$  was the peak height and FWHM the full width at half maximum. The  $S$  factor was strongest for the dominant drift mode A (61.8) and considerably weaker in mode C (16.5). We have also measured the average separation between the subpulses,  $P_2$ , in each of the drifting states using auto-correlation across the pulse longitude and subsequently averaging them for all relevant single pulses. The  $P_2$  also varied in the three drift states with minimum separation of  $7.6 \pm 0.1^\circ$  in longitude for mode C. The corresponding value in mode A was  $8.3 \pm 0.1^\circ$  which changed to  $9.1 \pm 0.1^\circ$  in the transition state before nulling. The fluctuation spectra in the disorderly mode B also shows some wide signal below frequencies of  $0.2 \text{ cy}/P$ . However, there was no clear frequency peak seen in this emission state. At certain short intervals the single pulse sequences during this mode also showed subpulse variations with periodicities seemingly less than mode A. This signifies that the pulse sequence during mode B had short bursts of drifting but no sustained ordered pattern. The different drifting periodicities and  $P_2$  values reported here differ from the drift mode esti-

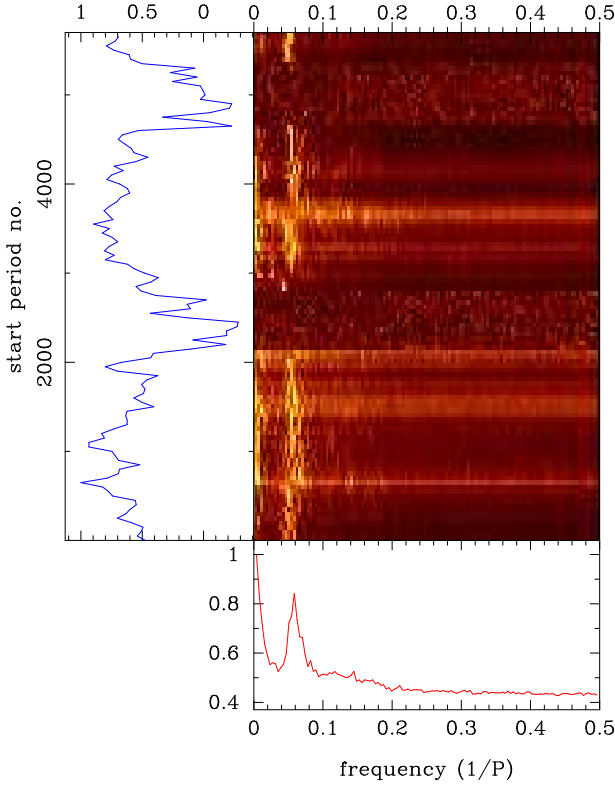


**Figure 4.** The figure shows the variation of the average Longitude Resolved Fluctuation spectra (LRFS) as a function of the start period. The LRFS is determined for 256 consecutive single pulses at a time. The starting point is shifted by 50 periods and the process is continued till the end of the observing duration. The average LRFS is calculated for each realization and is represented in the colour plot as a function of the starting period. The average across the x-axis is shown on the left window while the average across the y-axis corresponding to the time average LRFS is shown on the bottom window. The time average LRFS exhibits two clear peak frequencies. The first peak at zero frequency can be attributed to nulling while the second peak corresponds to the subpulse drifting in the dominant mode A. The figure also shows the two intervals during phasing of the antennas where the corresponding LRFS has been replaced with noise.

**Table 2.** Characterising the nulling in PSR J1822–2256.

$N_P$	$NF$ (%)	$N_T$	$\langle BL \rangle$	$\langle NL \rangle$	$P_N$ ( $P$ )
5693	$5.5 \pm 0.2$	211	26.0	2.1	$134 \pm 33$

mates reported in [Naidu et al. \(2017\)](#) for this pulsar. The different drift periodicities in this earlier work were estimated from average fluctuation spectra involving 256 periods. Our analysis showed that all emission states have much shorter durations and their behaviour would be diminished in these longer integration studies which may lead to erroneous measurements.

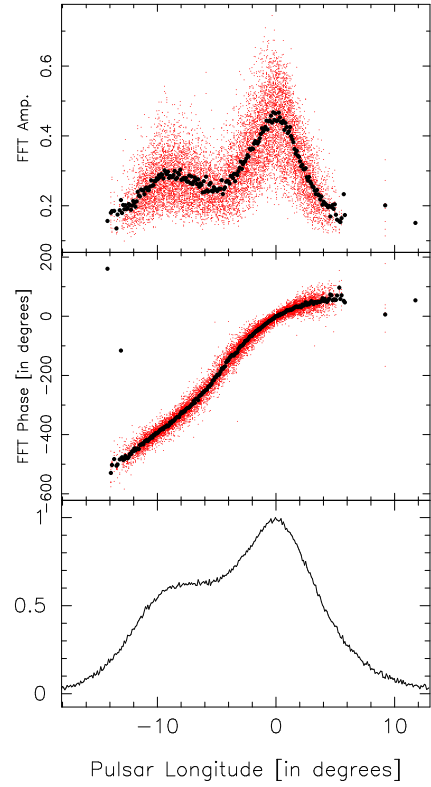


**Figure 5.** The figure shows the variations of the peak amplitude (top window) and the phase (middle window) of the Longitude Resolved Fluctuation spectra (LRFS) across the pulse profile. The average profile shape is shown in the bottom window. The LRFS is determined for 256 consecutive single pulses at a time. The starting point is shifted by 50 periods and the process is continued till the end of the observing duration. In each case the peak amplitude represents the subpulse drifting in mode A. The spread of the peak amplitude and phase, represented by red points, corresponds to their variations with time while the black dots are the average values at each longitude. The amplitude variations resemble the profile shape. The phase variations are non-linear with the trailing part flatter than the leading part.

## 4 NULLING

The nulling in the pulsar J1822–2256 was previously reported in [Basu et al. \(2017\)](#); [Naidu et al. \(2017\)](#). [Basu et al. \(2017\)](#) suggested that the presence of the low frequency peak in the fluctuation spectra was a manifestation of periodic nulling which is only seen in around twenty pulsars. The presence of periodic nulling along with subpulse drifting in the same pulse sequence is even more rare and was previously reported in six other pulsars. This was a primary motivation for [Basu et al. \(2017\)](#) to suggest the two phenomena to have different physical origin. We followed the analysis schemes detailed in [Basu et al. \(2017\)](#) to estimate the nulling properties. The primary analyses to characterize nulling are shown in figure 7 which include the energy distributions in the on-pulse window as well as the off-pulse region (top panel), the null and burst length histograms (middle panels) and the separate folded profiles of null and burst pulses (bottom plot). The details of nulling are also summarized in table 2. The nulling fraction ( $NF$ ) was  $5.5 \pm 0.2$  percent which is consistent with the measurements of [Basu et al. \(2017\)](#), which had shorter observing durations, but is different from the  $10 \pm 2$  percent reported in [Naidu et al. \(2017\)](#). We have measured 211 transitions ( $N_T$ ) from the burst state to the null state and vice versa. The null states were dominated by shorter duration nulls as

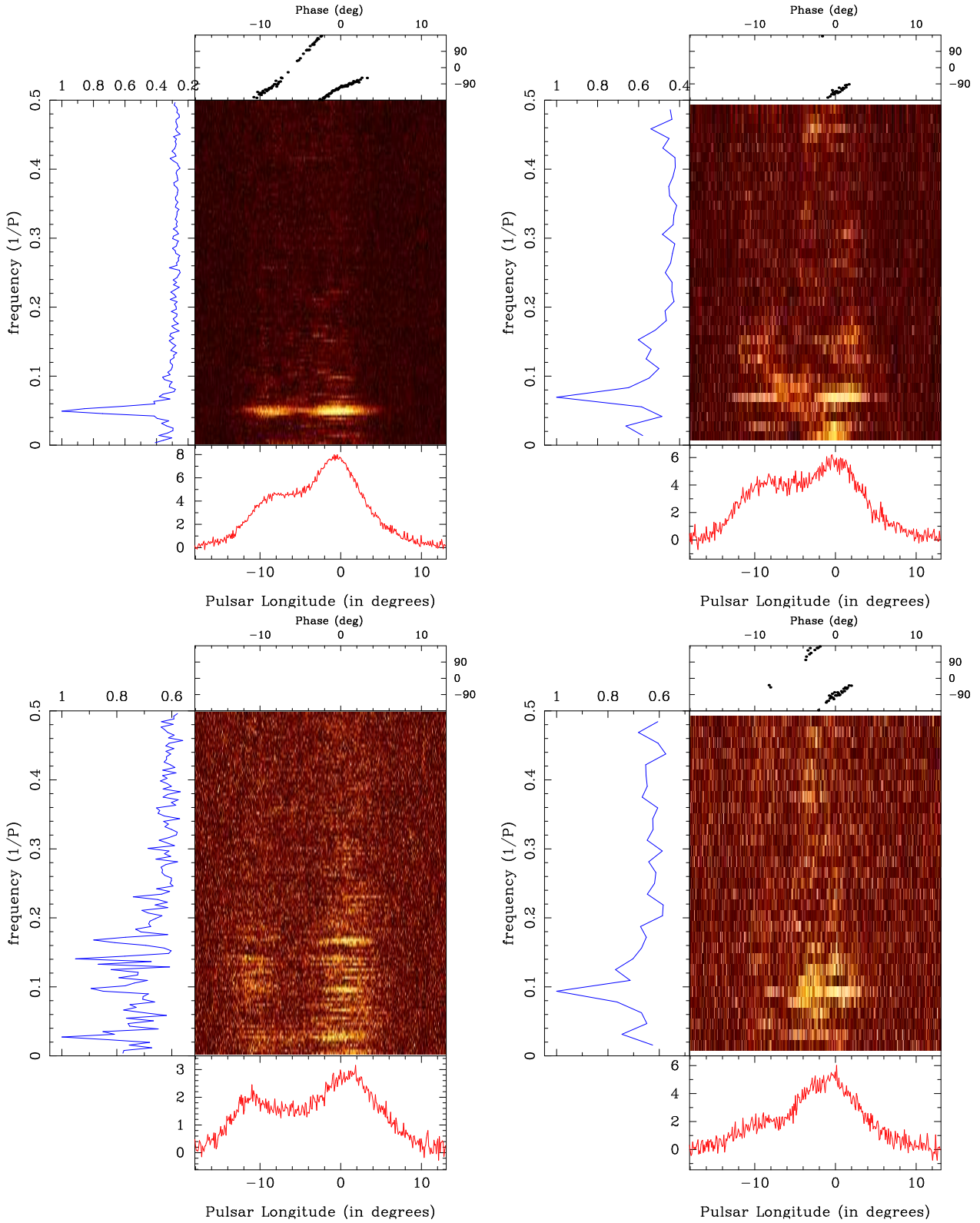


**Figure 6.** The figure shows the Longitude Resolved Fluctuation Spectra (LRFS) for four different single pulse sequences corresponding to mode A (top left), the transitional drifting state before the onset of nulling in mode A (top right), the disorderly mode B (bottom left) and the drifting mode C (bottom right). The LRFSs show the drifting to be present throughout the pulse window in the first two cases but only near the trailing edge in mode C. In contrast no clear drifting peak is seen in mode B. However, a wishy structure can be discerned below 0.2 cycles/ $P$  indicating disordered subpulse motion during this mode. The drifting periodicities are  $19.6 \pm 1.6 P$  in mode A,  $14.3 \pm 1.8 P$  during the transition to nulls in mode A and  $10.7 \pm 1.1 P$  in mode C which do not seem to be harmonically related to each other.

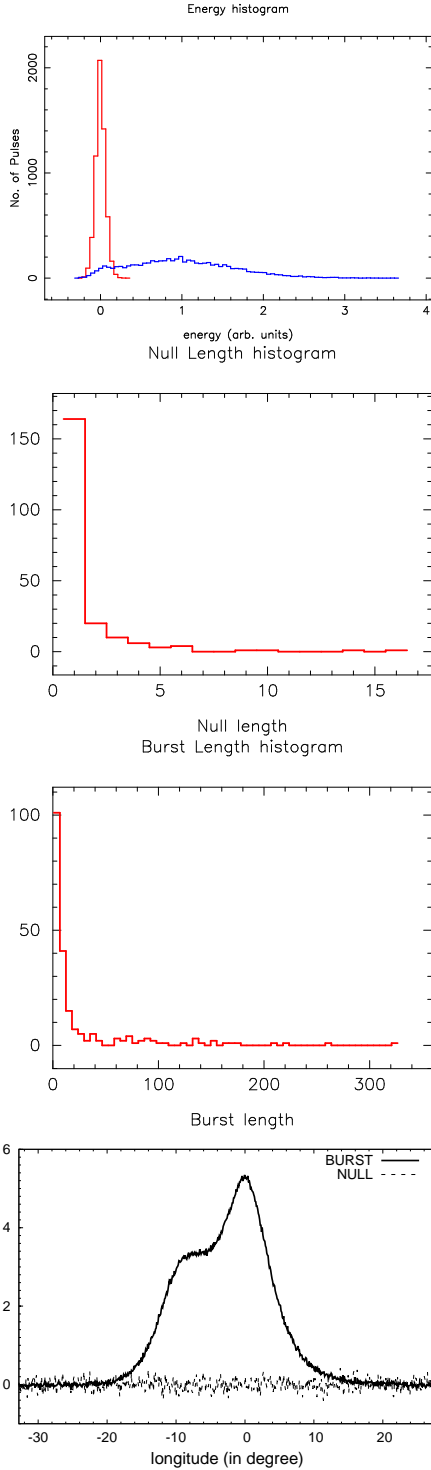


**Figure 7.** The figure shows the different analyses to characterise the nulling in the pulsar J1822–2256. The top panel shows the histograms corresponding to the average energy distribution, in arbitrary units, in the on-pulse window (blue) as well as the noise distribution from an off-pulse window (red), which resembles a Gaussian function centered around zero. The on-pulse energies show a peak around zero which correspond to the null pulses. The two central panels show the null length and burst length histograms for the pulse sequence. The nulls are of short duration and mostly last for one or two periods. Finally, the bottom plot shows the folded profiles for the null and burst pulses separately. The null profile is noise like and does not show any pulsed signal which validates our identification scheme for nulling.

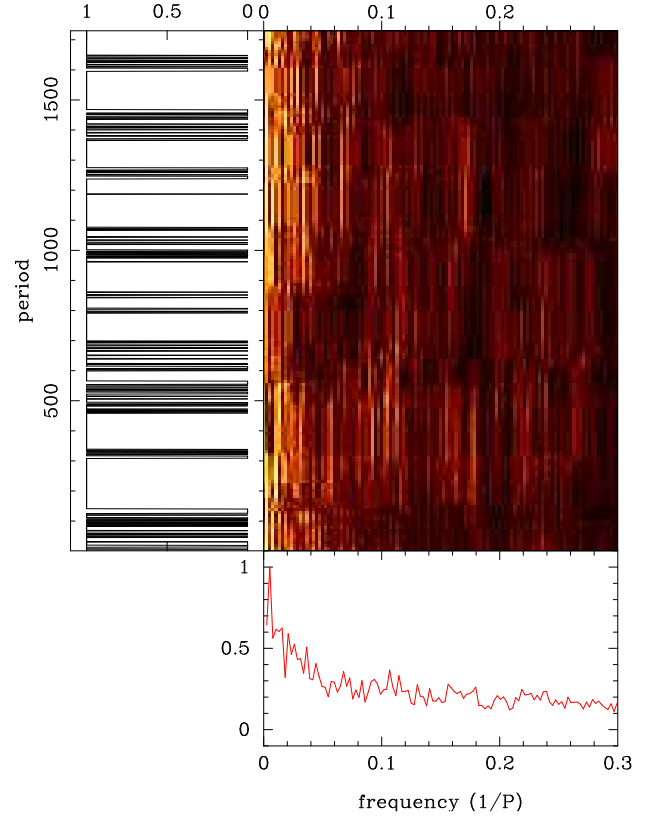


**Figure 8.** The figure shows the zoomed in (along x-axis) FFT for the Null/Burst sequence where the nulls have been replaced with ‘0’ and bursts with ‘1’. The nulling periodicity was estimated using an FFT length of 512 periods at a time. The starting period was shifted by ten periods and the process was repeated to estimate the time variations in the nulling periodicity.

seen in the null length histogram. The average null length ( $\langle NL \rangle$ ) was around two periods. The burst lengths on the other hand were of much longer durations reaching a maximum of around 300 consecutive periods and an average length ( $\langle BL \rangle$ ) of around 26 periods.

The zero frequency structure in the average LRFS (Fig. 8) was likely associated with nulling. Given the long duration of observations we explored the possibility of resolving this periodicity by using longer duration FFT studies and firmly associating the periodicity with the nulling process. We used the null/burst sequence FFT as described in Basu *et al.* (2017), where the nulls were replaced with ‘0’ and bursts with ‘1’ to produce a time series of binary numbers. An FFT of this sequence was carried out to estimate the periodicity of nulling. We have experimented with varying FFT lengths and finally used 512 periods which enabled us to clearly separate the peak frequency from the zero boundary. The starting position was shifted by ten periods and the FFT was repeated till the end of the observing duration to determine the time variations as shown in figure 8. A time averaged FFT was estimated and used to calculate the nulling periodicity. Our analysis clearly demonstrates that the low frequency structure seen in the LRFS corresponds to nulling. The corresponding periodicity ( $P_N$ ) was calculated to be  $134 \pm 33P$ .

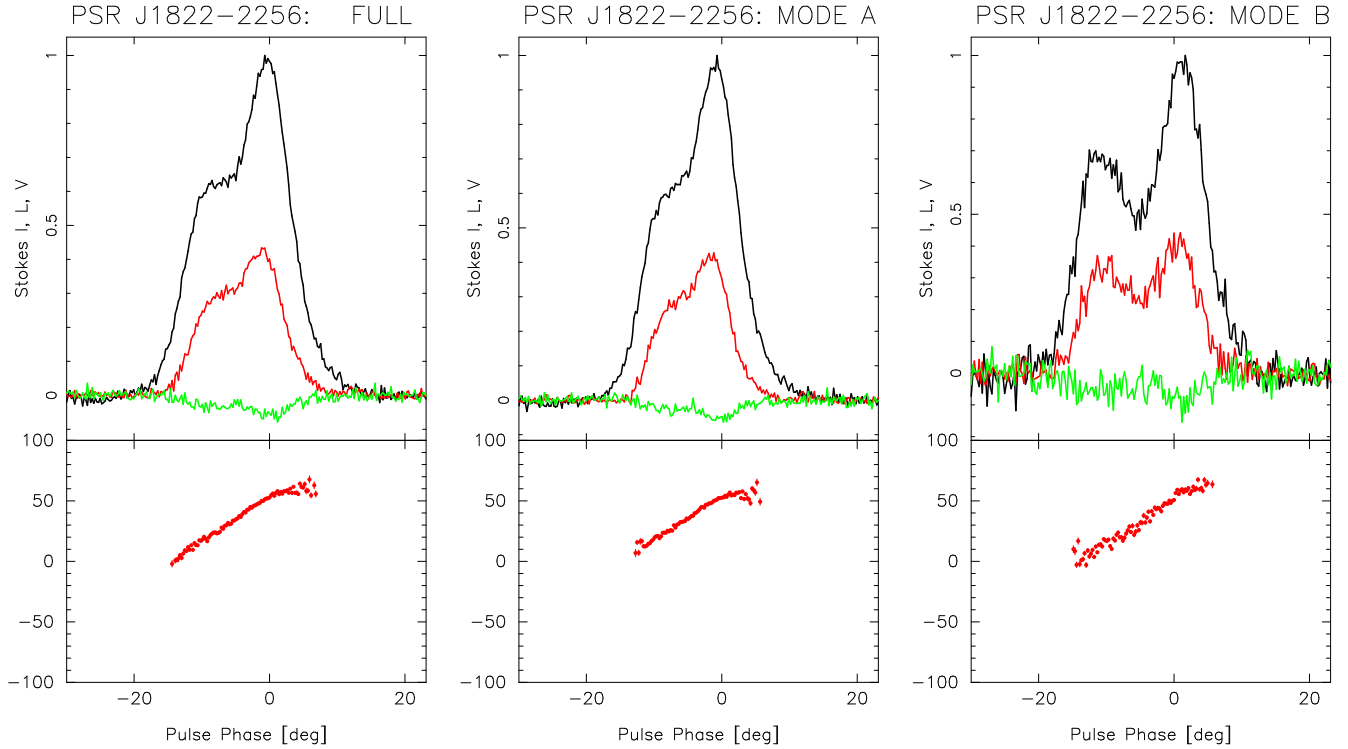


**Figure 9.** The figure shows the average polarization properties of the pulsar J1822–2256 corresponding to the full observing session (left panel), Mode A (middle panel) and Mode B (right panel). The polarization information was recorded in the shorter duration MSPES studies (Mitra *et al.* 2016). We could only distinguish the two prominent modes A and B from these observations. The top window in each plot shows the average profile (black line) along with the linear polarization (L, red line) and the circular polarization (V, green line). The fraction of linear polarization varies slightly in the two modes. The bottom window in each figure shows the polarization position angle (PPA). The PPA is identical within measurement errors for all three cases.

**Table 3.** Emission Properties at different Modes.

Mode	$W_{3\sigma}$ ( $^{\circ}$ )	$W_{10}$ ( $^{\circ}$ )	%L	%V
Full.	$35.7 \pm 0.5$	$25.0 \pm 0.5$	$38.1 \pm 0.4$	$-5.3 \pm 0.4$
Mode A	$35.4 \pm 0.5$	$22.7 \pm 0.5$	$35.6 \pm 0.4$	$-4.2 \pm 0.4$
Mode B	$35.6 \pm 0.5$	$28.6 \pm 0.5$	$39.1 \pm 1.0$	$-8.0 \pm 2.0$
Mode C	$25.3 \pm 0.5$	$22.3 \pm 0.5$	—	—

## 5 DISCUSSION

### 5.1 The Emission Region

The subpulse drifting is a result of the dynamics of the sparking discharges in the IAR characterised by large non-dipolar magnetic fields. The radio emission on the other hand originates at heights of few hundred kilometers above the stellar surface which are dominated by dipolar magnetic field lines. The presence of multiple drifting states and mode changing gives an unique opportunity to investigate if these changes have a corresponding effect on the emission process as well, primarily the emission altitudes.

The characterisation of the pulsar geometry as well as the location of the radio emission require polarimetric observations (see Mitra 2017, for a review). The polarization position an-

gle (PPA) across the pulse window shows a characteristic S-shape curve. The PPA is interpreted using the Rotating Vector Model (RVM, Radhakrishnan & Cooke 1969) where the radiation is highly beamed and arises from regions of dipolar diverging field lines. The S-shaped curve is formed as the line of sight traverses across the diverging field lines. The pulsar geometry is characterised by  $\alpha$ , the angle between the rotation axis and the dipolar magnetic axis, and  $\beta$ , the angle between the rotation axis and the observers' line of sight. A relation between the steepest gradient (SG) point of the PPA and the pulsar geometry can be estimated using the RVM as  $SG = \sin(\alpha) / \sin(\beta)$ . It has been observed that correlations exist between the profile type and the shape of the PPA (Rankin 1993). For a highly central cut of the emission beam the SG points of the PPA traverse is large and the profile has multiple components with core and conal emission. As the observer cuts the emission beam more tangentially the SG is less steep and the profile shape varies from a double to a single component. Detailed beam shape studies have revealed that the average emission beam comprises of nested cones around a central core emission region (Mitra & Deshpande 1999).

The phase-modulated subpulse drifting, as seen in PSR J1822–2256, is usually associated with conal profiles with shallow PPA traverses. The profile shapes of these pulsars also show an evolution with frequency where low frequency double profiles usually become single component profiles at very high frequencies (Rankin 1993). Hence, average profiles at multiple frequencies are required to classify the profile type. We did not find any previous classification for the pulsar J1822–2256 in the literature. However, average profiles at multiple frequencies were available from an archival

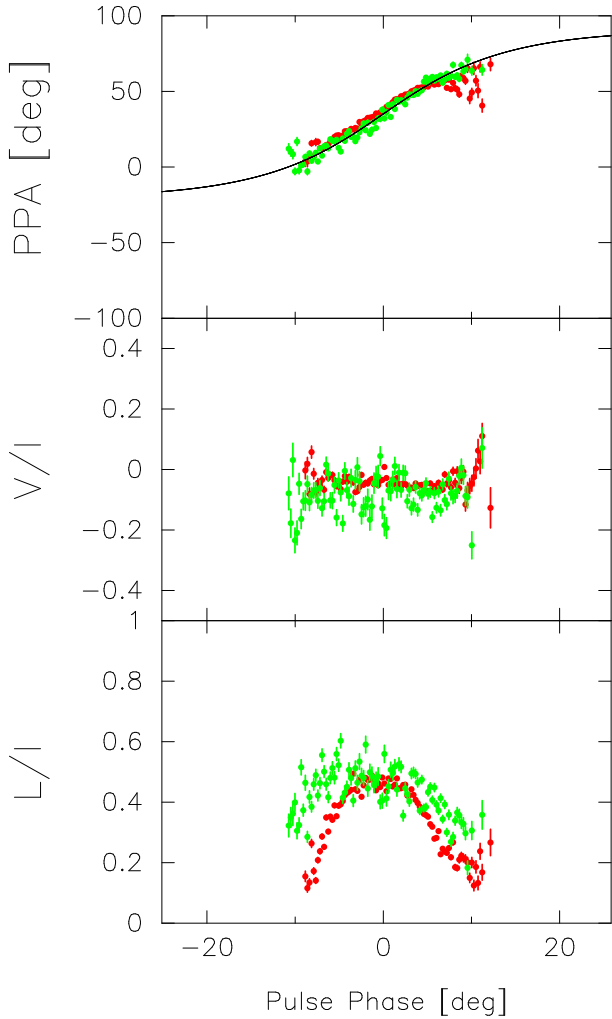


**Figure 10.** The figure shows the comparison of the polarization properties across the pulse window for the two emission modes A (in red) and B (in green). The top window shows the polarization position angle (PPA) in the two modes. A realization of the rotating vector model (RVM, black line) is also shown which accurately fits the PPA in the two modes. The phase center of the RVM is located at  $-4.37^\circ$  longitude compared to the profile peak and we have shifted the plots to coincide with the phase center. The middle window shows the fractional circular polarization ( $V/I$ ) at each pulse longitude. The bottom window shows the fractional linear polarization ( $L/I$ ) at each pulse longitude.

database<sup>1</sup>. Additionally, we also used the polarization observations from MSPES to estimate its emission properties. The left panel of figure 9 shows the polarization behaviour for the average profile at 333 MHz. The PPA traverse is relatively shallow with estimated SG =  $4.0^\circ$ . This is indicative of a tangential line of sight cut of the emission beam. The average profiles of this pulsar also show a single component at higher frequencies (for example at 4.85 GHz). We conclude that the profile classification for this pulsar is consistent with conal single type.

Next we proceed to compare the emission region in the different modes. The average profiles in the three primary modes (see figure 2) show very different shapes. However, comparison with the complete pulsar profile in each case (shown as dot dashed line

in figure 2) suggests that the widths remain largely unchanged for the three modes. We have estimated the widths at three times the rms level of the baseline ( $W_{3\sigma}$ ) as well as the ten percent of the peak height ( $W_{10}$ ) as shown in table 3. The  $W_{3\sigma}$  were identical for modes A and B. Due to higher baseline noise levels the estimated  $W_{3\sigma}$  was lower for the profile in mode C. However, the  $W_{10}$  in this case was once again identical to mode A. This signifies that in the different modes the emission regions were bounded by similar points along the open field lines. We could only identify the modes A and B in the MSPES observations and determined their average polarization behaviour as shown in figure 9 (middle and left panel, respectively). Additionally, we have also carried out comparisons of the PPA traverse, the linear and circular polarization across the pulsar profile for the two modes as shown in figure 10 (mode A in red and mode B in green). The PPA traverses (top panel) were identical for the two modes with the same RVM (black line) fitting both of them. The RVM fit shown in the figure corresponds to  $\alpha = 16.2^\circ$  and  $\beta = 4.0^\circ$ <sup>2</sup>. Mode B seemed to have slightly higher linear polarization towards the leading and trailing part of the profile but no discernible difference in circular polarization could be seen in the two modes. Such slight variations in fractional polarization can be associated with changes in plasma inhomogeneity (Melikidze *et al.* 2014). These analyses show that during the mode changes the emission region remains largely unaffected and the emission continues to arise from the same heights.

The radio emission arises due to non linear plasma processes where charged bunches (relativistic solitons) excite coherent curvature radiation in curved magnetic fields. The emission from a large number of such charged bunches adds up incoherently to give the observed radio intensity (Asseo & Melikidze 1998; Melikidze *et al.* 2000; Gil *et al.* 2004). In such a model the characteristic frequency of emission ( $\nu_c$ ) is given as  $\nu_c \sim \gamma^3 c / \rho_c$ , where  $\gamma$  is the Lorentz factor of the radiating plasma and  $\rho_c$  is the underlying radius of curvature of the magnetic field. As argued above that during mode transitions the geometry remains unchanged which implies that  $\rho_c$  across the emission region is also unchanged for the three modes. This further suggests that in order to get the same  $\nu_c$ , the  $\gamma$  of the radiating plasma also needs to be similar in the different modes. The power of the radio emission in this model is  $P \propto F(Q)\gamma^4 / \rho_c^2$ , where  $F(Q)$  has the dimension of charge squared and is a complex function of the plasma parameters. The observations show that despite the emission geometry remaining same across the profile, the emitted power at different longitudes varies in the three modes. This can only arise due to variation in the  $F(Q)$  which depends on the changes in the plasma parameter in a complicated manner. Similar conclusions have also been drawn for the mode changing pulsar PSR B0329+54 where observations revealed that the locations of the radio emission were similar for the different modes (Bartel *et al.* 1982, Brinkman, Mitra & Rankin, 2017, private communication). The plasma changes are likely driven by variations in the IAR where they are generated. In summary, our analyses reveal that the variations seen during mode changing are unlikely to be affected by changes in the emission region and are possibly driven by the complex plasma processes which take place during their generation in the IAR.

<sup>2</sup> Fitting the RVM to the PPA gives estimates of the angles  $\alpha$  and  $\beta$ . However, these estimates are highly correlated and do not give good constraints on the geometry. Rather the SG point is significantly better determined in the PPA traverse.

<sup>1</sup> EPN pulsar Database

## 5.2 Variations in Subpulse Drifting during Mode Changing

The presence of multiple drifting states in addition to a disorderly mode and periodic nulling in the same pulsar gives an unique opportunity to further investigate the physical conditions in the magnetosphere. As argued in the previous section the emission regions for different modes are similar and the mode changing is driven by variations in the IAR. In this regard the presence of different drifting properties is useful to better understand the conditions in the IAR. The sparks in the IAR responsible for the generation of the outflowing plasma have typical timescales ranging from hundreds of nanoseconds to microseconds (Ruderman & Sutherland 1975, hereafter RS75). These are much shorter than the drifting periodicities which represent average behaviour of the conditions in the IAR. The drifting periodicity can be estimated as  $P_3 = d/v_d$ , where  $d$  is the average separation between two consecutive sparks and  $v_d$  the drift velocity of the sparks. In the IAR  $v_d$  can be further expressed as  $v_d = (\Delta E/B)c$ , where  $\Delta E$  is the change in the electric field in the gap during the sparking process,  $B$  the magnetic field in the IAR and  $c$  the speed of light. It is difficult to see how the magnetic field associated with the star can change at these timescales since this will result in large scale reorientation of the current flow in the pulsar circuit (Spitkovsky 2011). Hence, the different  $P_3$  values can be attributed to either changes in  $d$  or  $\Delta E$  or combinations of both, i.e. on the term  $d/\Delta E$ . The separation between the sparks can be approximately related to  $P_2$  and the pulsar geometry as  $d \propto 2\pi \left(\frac{P_2}{360^\circ}\right) \sqrt{\frac{R_S^3}{R_E}} \sin(\alpha + \beta) b^{0.5}$ . Here,  $R_S$  is the radius of the neutron star,  $R_E$  the height of the emission region and  $b$  the scaling factor between dipolar component and the non-dipolar field in the IAR. As reported earlier the three drifting states have different  $P_2$  values. We have argued above that the emission geometry and  $R_E$  in the three modes are similar. This implies that the  $P_2$  variations in the emission region are indicative of changes in the spacing between sparks. Hence, the number of sparks in the IAR are different in each emission mode. According to RS75 the sparking process is governed by the energy of background  $\gamma$ -ray photons and the IAR electric field  $\Delta E$ . A change in  $P_2$  is a direct indication that the  $\Delta E$  in the gap is also changing. There are however no provisions for such changes in the steady state models like RS75.

As noted earlier mode changing, nulling and drifting phenomena occur on timescales which are significantly larger than the dynamics of the plasma formation. This has also been recognized in earlier observations of mode changing where external mechanisms were expected to change the plasma flow during the changes (Bartel *et al.* 1982). In several recent studies (Basu *et al.* 2016, 2017; Mitra & Rankin 2017; Rajwade *et al.* 2017) the mode changing and nulling phenomena have been reported to have a periodic/quasi-periodic nature. It was suggested by Basu *et al.* (2017) that an external triggering mechanism in the larger magnetosphere is required to drive the periodic changes in the plasma generation process of the IAR. In this work we show the presence of periodic nulling as well as regular mode changing in the same system. The nulling periodicity is  $134 \pm 33 P$ . The pulsar primarily exists in the two modes A and B. We found the average duration of mode A to be 82 periods and that of mode B to be 68 periods. This means that on average the pulsar comes back to its initial mode at a timescale of  $150 (82+68) P$ , which is comparable to the nulling periodicity. This prompts the interesting possibility that the triggering mechanism proposed earlier for the periodic nulling phenomenon

also induces the mode changing in this pulsar. However, the physical origin of the triggering mechanism is unknown.

The different drifting states associated with the emission modes have been investigated in the past using the carousel model. The significant frequency evolution of profile widths in J1822–2956 suggests the presence of outer cone which has been argued to have a beam radius,  $\rho = 5.75^\circ/P^{0.5} \approx 4.2^\circ$  (Rankin 1993). The number of circulating beamlets in the different drifting states can be estimated using  $\rho$  and the corresponding  $P_2$  values (Deshpande & Rankin 2001). It was argued by Rankin *et al.* (2013) that in the pulsar B1918+19 the carousel circulation time was constant across the different drifting modes. The number of subbeams making up the circulation pattern changed in the different drifting states leading to the difference in the measured  $P_3$ . It is possible to extend these analysis schemes for the drifting modes of J1822–2956 as well, but recent observations have raised questions about the applicability of carousel model in pulsars (Basu *et al.* 2016; Mitra & Rankin 2017). The preponderance of short duration nulls known as ‘pseudo nulls’, seen periodically, as reported here for the pulsar J1822–2956 has been used as additional justification for the carousel model (Herfndal & Rankin 2007, 2009). The pseudo nulls are associated with the line of sight passes across the empty regions within the rotating subbeam system. However, the presence of pseudo nulls reported in core dominated pulsars challenges this interpretation (Basu *et al.* 2017).

Another possibility for the mode changing and nulling has been suggested by Timokhin (2010). In this model the transitions to the emission states are governed by corresponding variations in the global magnetospheric current flow which can change the extent of the open field line regions. A possible observational indication is difference in the profile widths and geometries in the different modes. However, similar widths of the profiles as well as the geometries for the three modes argue against the model to be applicable in this pulsar.

## 6 SUMMARY

We have carried out detailed analyses of the single pulse dynamics in the pulsar J1822–2256. We have identified several distinct emission states and have categorized them as three different modes based on their relative abundances. The most dominant mode seen for around 45 percent times was identified as mode A. This mode consisted of prominent drift bands seen across the entire profile from the leading to the trailing edge. Mode B was seen for around 38 percent of the observing duration and was more disorderly without the presence of any clear subpulse drifting. A third mode C is comprised of a second drift mode with periodicity lower than mode A. The emission state was seen for a single interval lasting for around 200 consecutive periods and was more bright towards the trailing part of the profile. In addition to the three distinct modes the pulsar also showed the presence of nulling throughout the observing durations. The nulling was present in all the states but was more frequent during the disorderly mode B. In some cases the drifting behaviour in mode A just before the onset of nulls changed, showing a periodicity different from both modes A and C. We have also shown the nulling to exhibit periodicity which is much larger than the drifting periodicities. The radio emission in this pulsar is unique owing to the diversity of single pulse phenomena seen in the same system. We have shown that the emission region remains unchanged in the three modes and the mode changing is likely driven by variation in the plasma generation process.

The regular change in the emission process cannot be explained using a conventional steady state model of plasma generation. Additional triggering mechanism from the pulsar magnetosphere would be required to change the plasma processes periodically/quasi periodically. This requires more detailed modelling which can then be constrained using the detailed observational inputs which have been gathered in recent works. Recent studies also show the radio mode changes have corresponding changes in the X-ray flux (Hermsen *et al.* 2013). This also indicates a change in the plasma generation process during mode changing.

## ACKNOWLEDGMENTS

We thank the referee Joanna Rankin for her comments which helped to improve the paper. We thank George I. Melikidze for discussions about subpulse drifting. We thank the staff of the GMRT who have made these observations possible. The GMRT is run by the National Centre for Radio Astrophysics of the Tata Institute of Fundamental Research.

## REFERENCES

- Asseo, E.; Melikidze, G.I. 1998, MNRAS, 301, 59  
 Backer, D.C. 1973, ApJ, 182, 245  
 Backer, D.C.; Rankin, J.M.; Campbell, D.B. 1975, ApJ, 197, 481  
 Bartel, N.; Morris, D.; Sieber, W.; Hankins, T.H. 1982, ApJ, 258, 776  
 Basu, R.; Mitra, D.; Melikidze, G.I.; Maciesiak, K.; Skrzypczak, A.; Szary, A. 2016, ApJ, 833, 29  
 Basu, R.; Mitra, D.; Melikidze, G.I. 2017, ApJ, 846, 109  
 Basu, R.; Mitra, D. 2018, accepted in MNRAS, eprint arXiv:1801.06038  
 Deich, W.T.S.; Cordes, J.M.; Hankins, T.H.; Rankin, J.M. 1986 ApJ, 300, 540  
 Deshpande, A.A.; Rankin, J.M. 2001, ApJ, 322, 438  
 Gil, J.; Lyubarsky, Y.; Melikidze, G.I. 2004, ApJ, 600, 872  
 Hankins, T.H.; Wolszczan, A. 1987, ApJ, 318, 410  
 Herfindal, J.L.; Rankin, J.M. 2007, MNRAS, 380, 430  
 Herfindal, J.L.; Rankin, J.M. 2009, MNRAS, 393, 1391  
 Hermsen, W.; Hessels, J. W. T.; Kuiper, L. *et al.* 2013, Science, 339, 436  
 Huguenin, G.R.; Taylor, J.H.; Troland, T.H. 1970, ApJ, 162, 727  
 Kloumann, I.M.; Rankin, J.M. 2010, MNRAS, 408, 40  
 McSweeney, S.J.; Bhat, N.D.R.; Tremblay, S.E.; Deshpande, A.A.; Ord, S.M. 2017, ApJ, 836, 224  
 Melikidze, G.I.; Gil, J.A.; Pataraya, A.D. 2000, ApJ, 544, 1081  
 Melikidze, G.I.; Mitra, D.; Gil, J.A. 2014, ApJ, 794, 105  
 Mitra, D., Deshpande, A.A. 1999, A&A, 346, 906  
 Mitra, D.; Gil, J.; Melikidze, G. 2009, ApJL, 696, L141  
 Mitra, D.; Basu, R.; Maciesiak, K.; Skrzypczak, A.; Melikidze, G.I.; Szary, A.; Krzeszowski, K. 2016, ApJ, 833, 28  
 Mitra, D.; Rankin, J. 2017, ApJ, 468, 4601  
 Mitra, D. 2017, JApA, 38, 52  
 Naidu, A.; Joshi, B.C.; Manoharan, P.K.; KrishnaKumar, M.A. 2017, A&A, 604, 45  
 Radhakrishnan, V.; Cooke, D.J. 1969, ApL, 3, 225  
 Rankin, J.M.; Wright, G.A.E.; Brown, A.M. 2013, MNRAS, 433, 445  
 Rankin, J.M. 1993, ApJ, 405, 285  
 Rajwade, K.; Seymour, A.; Lorimer, D.R.; Karastergiou, A.; Serylak, M.; McLaughlin, M.A.; Griessmeier, J.-M. 2017, MNRAS, 462, 2518  
 Redman, S.L.; Wright, G.A.E.; Rankin, J.M. 2005, MNRAS, 357, 859  
 Ruderman, M.A.; Sutherland, P.G. 1975, ApJ, 196, 51  
 Serylak, M.; Stappers, B. W.; Weltevrede, P. 2009, A&A, 506, 865  
 Smits, J.M.; Mitra, D.; Kuijpers, J. 2005, A&A, 440, 683  
 Spitkovsky, A. 2011, ASSP, 21, 139  
 Sturrock P.A. 1971, ApJ, 164, 529  
 Swarup, G., Ananthakrishnan, S., Kapahi, V. K., et al. 1991, CuSc, 60, 95

- Timokhin, A. 2010, MNRAS, 408, 41  
 Vivekanand, M.; Joshi, B. C. 1997, ApJ, 477, 431  
 Weltevrede, P.; Edwards, R. T.; Stappers, B. W. 2006, A&A, 445, 243  
 Weltevrede, P.; Edwards, R. T.; Stappers, B. W. 2007, A&A, 469, 607  
 Wright, G.A.E.; Fowler, L.A. 1981, MNRAS, 101, 356